12-2008

Hydraulic Actuated Automotive Cooling Systems - Nonlinear Control and Test

John Wagner
Clemson University, jwagner@clemson.edu

M H. Salah
Clemson University

P M. Frick
General Electric Energy

D M. Dawson
Clemson University

Control Engineering Practice 17 (2009) 609–621

Contents lists available at ScienceDirect

Control Engineering Practice

journal homepage: www.elsevier.com/locate/conengprac

Hydraulic actuated automotive cooling systems—Nonlinear control and test

M.H. Salah [a], P.M. Frick [b], J.R. Wagner [c,*], D.M. Dawson [d]

[a] Department of Mechatronics Engineering, Hashemite University, Zarqa, Jordan
[b] General Electric Energy, Greenville, SC, USA
[c] Department of Mechanical Engineering, Clemson University, Clemson, SC, USA
[d] Department of Electrical Engineering, Clemson University, Clemson, SC, USA

ARTICLE INFO

Article history:
Received 3 December 2007
Accepted 17 October 2008
Available online 13 December 2008

Keywords:
Hydraulic
Automotive
Cooling
Nonlinear control

ABSTRACT

The replacement of traditional automotive mechanical cooling system components with computer controlled servo-motor driven actuators can improve temperature tracking and reduce parasitic losses. The integration of hydraulic actuators in the engine cooling circuit offers greater power density in a smaller package space when compared with electric actuators. In this paper, a comprehensive nonlinear backstepping robust control technique is developed to regulate the engine coolant temperature by controlling a hydraulic coolant pump and radiator fan. An experimental test bench has been assembled to investigate the hydraulic automotive thermal system performance. Representative numerical and experimental results are presented and discussed. Overall, the proposed controller was successful in tracking prescribed engine temperature profiles while harmoniously regulating the power consumption of the coolant pump and radiator fan.

1. Introduction

Traditional automotive cooling systems have relied on a mechanical coolant pump and a radiator fan driven off the engine's crankshaft. The dependence of the pump and fan operations on the engine speed often allowed the thermal management system to overcool the fluid, thus, decreasing the overall efficiency (Wambsganss, 1999). Advanced automotive cooling system designs replace the conventional wax-based thermostat valve with a variable position smart valve, and upgrade the mechanical coolant pump and radiator fan with computer controlled servo-motor actuators (Choukroun & Chanfreau, 2001; Wagner, Paradis, Marotta, & Dawson, 2002). Recent attention has focused on electric actuators to drive the cooling system components (Allen & Lasecki, 2001) with possible thermal management opportunities in HCCI applications (Shaver, Roelle, & Gerdes, 2006) using a coolant rail (Chastain & Wagner, 2006). However, an opportunity exists to introduce hydraulic-driven motors to power these variable speed cooling components and leverage the attractive hydraulic properties such as power density and compact packaging (Dostal, 1994). For large displacement engines (e.g., buses, heavy duty trucks), the power requirements for the coolant pump and radiator fan increase significantly when compared to passenger vehicles. For electric motors to meet these requirements, they are required to be either a large single motor or applied in a distributed manner with multiple motors.

A variety of mathematical models have been presented for automotive thermal management system and hydraulic-driven components. Vaughan and Gamble (1996) proposed a nonlinear model for hydraulic solenoid valves. Havlicsek and Alleyne (1999) developed a dynamic model that included stick-slip friction, time delays, nonlinear valve flow characteristics, and deadzones for electro-hydraulic equipment. Yao, Bu, Reedy, and Chiu (2000) investigated electro-hydraulic single-rod actuated systems and considered system nonlinearities and parametric uncertainties in the analytical model. Henry, Koo, and Richter (2001) developed and validated an automotive powertrain cooling system model for light duty truck applications. Finally, Frick, Bassily, Watson, and Wagner (2006) created a series of mathematical models that described hydraulic driven heat exchanger for automotive cooling applications.

To control the thermal management system components (e.g., Setlur, Wagner, Dawson, & Marotta, 2005) and to operate hydraulic-driven actuators (e.g., Chiang, Lee, & Huang, 2005), different control architectures and operating strategies have been proposed. Hamamoto, Omura, Ishikawa, and Sugiyama (1990) developed an electronically controlled hydraulic cooling fan system which identified the optimum fan speeds per engine operating conditions. Liu and Alleyne (2000) created a Lyapunov-based nonlinear control algorithm which tracked the force and pressure of an electro-hydraulic actuator with a single-stage servo-valve. Yao, Bu, and Chiu (2001) proposed a discontinuous projection-based adaptive robust controller for an

* Corresponding author. Tel.: +1 864 656 7376; fax: +1 864 656 4435.
E-mail address: jwagner@clemson.edu (J.R. Wagner).

0967-0661/$ - see front matter © 2008 Elsevier Ltd. All rights reserved.
doi:10.1016/j.conengprac.2008.10.016

Nomenclature

a	solenoid contact length (mm)
b_{val}	hydraulic valve damping (N s/m)
B_m	hydraulic motor damping (N s/cm)
B_{mf}	hydraulic fan motor damping (N s/cm)
B_{mp}	hydraulic pump motor damping (N s/cm)
c_a	conversion constant (m^3/rad)
c_c	conversion constant (m^3/rad)
c_{pa}	air specific heat (kJ/kg K)
c_{pc}	coolant specific heat (kJ/kg K)
C_d	hydraulic motor damping coefficient
C_{df}	hydraulic fan motor damping coefficient
C_{dp}	hydraulic pump motor damping coefficient
C_e	engine block thermal capacity (kJ/K)
C_{im}	internal motor leakage coefficient (cm^5/N s)
C_{imf}	internal fan motor leakage coefficient (cm^5/N s)
C_{imp}	internal pump motor leakage coefficient (cm^5/N s)
C_r	radiator thermal capacity (kJ/K)
D_m	hydraulic motor displacement (m^3/rad)
D_{mf}	hydraulic fan motor displacement (m^3/rad)
D_{mp}	hydraulic pump motor displacement (m^3/rad)
f_L	nonlinear function to related the fluid mass flow rate with the load torque
F_s	force generated by the solenoid coil (N)
F_{ss}	steady-state fluid force on the solenoid (N)
F_{ss}^1	steady-state force due to fluid exiting the main valve chamber to port A (N)
F_{ss}^2	steady-state force due to fluid exiting port B to tank (N)
F_{tr}	transient fluid force on the solenoid (N)
F_{tr}^1	transient fluid force between loads A and B when spool displaced (N)
F_{tr}^2	transient fluid force to right of land B when spool displaced (N)
i	control valve coil current (A)
J	hydraulic motor and load inertia (kg cm^2)
J_f	hydraulic fan and load inertia (kg m^2)
J_p	hydraulic pump and load inertia (kg cm^2)
k_{val}	hydraulic valve spring constant (N/m)
l_g	solenoid valve reluctance gap (m)
L	control valve coil internal inductance (H)
L_d	damping length (m)
$\dot{m}_a$	fan air mass flow rate (kg/s)
$\dot{m}_c$	pump coolant mass flow rate (kg/s)
m_s	hydraulic valve spool mass (kg)
N_t	number of turns in solenoid coil
P_A	hydraulic motor supply pressure (kPa)
P_B	hydraulic motor return pressure (kPa)
P_L	hydraulic motor load pressure (kPa)
P_{Lf}	hydraulic fan motor load pressure (kPa)
P_{Lp}	hydraulic pump motor load pressure (kPa)
P_S	supply pressure (kPa)
P_{Sf}	hydraulic fan motor supply pressure (kPa)
P_{Sp}	hydraulic pump motor supply pressure (kPa)
P_{sys}	cooing system power consumption (W)
P_T	Tank pressure (kPa)
Q_{in}	combustion process heat energy (kW)
Q_L	hydraulic motor load flow (LPM)
Q_{Lf}	hydraulic fan motor load flow (LPM)
Q_{Lp}	hydraulic pump motor load flow (LPM)
Q_o	uncontrollable radiator heat losses (kW)
R	control valve coil internal resistance (Ω)
sgn	standard signum function
t	current time (s)
T_e	radiator inlet coolant temperature (K)
T_{ed}	desired engine temperature trajectory (K)
T_g	hydraulic motor generated torque (N cm)
T_L	hydraulic motor load torque (N cm)
T_{Lf}	hydraulic fan motor load torque (N cm)
T_{Lp}	hydraulic pump motor load torque (N cm)
T_r	radiator outlet coolant temperature (K)
T_{vr}	design virtual radiator reference temperature (K)
$\bar{T}_{vr}$	control input (K)
T_{vro}	min. virtual radiator reference temperature (K)
T_∞	surrounding ambient temperature (K)
u_e	pump speed control law (kJ rad/m^3 s)
u_f	hydraulic fan solenoid valve control law ((N s rad/cm^3) $\sqrt{\text{kPa m}^3/\text{kg}}$)
u_p	hydraulic pump solenoid valve control law ((N s rad/cm^3) $\sqrt{\text{kPa m}^3/\text{kg}}$)
u_r	fan speed control law (kJ rad/m^3 s)
V	control valve coil voltage (V)
V_t	volume of compressed fluid (cm^3)
V_{tf}	fan motor compressed fluid volume (cm^3)
V_{tp}	pump motor compressed fluid volume (cm^3)
w	orifice area gradient (cm^2/cm)
w_f	fan orifice area gradient (cm^2/cm)
w_p	pump orifice area gradient (cm^2/cm)
x	control valve spool displacement (m)
x_{mf}	fan valve max. spool displacement (m)
x_{mp}	pump valve max. spool displacement (m)
x_p	fan control valve spool displacement (m)
x_f	fan control valve spool displacement (m)
X_f	fan control valve spool displacement ratio
X_p	pump control valve spool displacement ratio
β	bulk modulus of hydraulic fluid (MPa)
β_f	bulk modulus of fan hydraulic fluid (MPa)
β_p	bulk modulus of pump hydraulic fluid (MPa)
ε	effectiveness of the radiator fan (%)
η_e	engine temperature tracking error (K)
η_{ess}	engine temperature steady-state error (K)
η_f	fan speed tracking error (rad/s)
η_p	pump speed tracking error (rad/s)
η_r	radiator temperature tracking error (K)
θ	temperature (K)
μ_0	solenoid armature permeability (H/mm)
ρ	fluid density (kg/m^3)
ρ_a	air density (kg/m^3)
ρ_c	coolant density (kg/m^3)
ρ_f	hydraulic fan fluid density (kg/m^3)
ρ_p	hydraulic pump fluid density (kg/m^3)
ω	hydraulic motor speed (rad/s)
ω_f	hydraulic radiator fan speed (rad/s)
ω_{fd}	designed desired fan speed (rad/s)
ω_p	hydraulic coolant pump speed (rad/s)
ω_{pd}	designed desired pump speed (rad/s)
ω_{po}	minimum coolant pump speed (rad/s)
$\bar{\omega}_{pd}$	control input (rad/s)

electro-hydraulic servo-system driven by double-rod hydraulic actuators. Chen, Dixon, Wagner, and Dawson (2002) developed a nonlinear backstepping exponential tracking controller for a hydraulic cylinder and proportional directional control valve to precisely position a mechanical load and accommodate inherent system nonlinearities. Lastly, Kaddissi, Kenné, and Saad (2007) created a nonlinear backstepping approach for the position control of an electro-hydraulic servo-system.

In this paper, a nonlinear backstepping robust controller will be developed to regulate the engine coolant temperature in a hydraulic-based automotive thermal management system. This control strategy was selected due to the system nonlinearities, need to accommodate system disturbances, and presence of plant uncertainties. The project's key contribution is to implement, for the first time, a hydraulic engine thermal management system with harmonious pump and fan control. In Section 2, the mathematical models are presented for the hydraulic-based thermal management system components. A backstepping robust tracking control strategy has been designed in Section 3. Section 4 contains the experimental test bench followed by representative numerical and experimental results in Section 5. The summary is presented in Section 6. Appendices A and B offer a standard Lyapunov-based stability analysis and the Nomenclature list.

2. Mathematical models

A suite of dynamic models describe the transient response of the hydraulic-based advance vehicle thermal management system. The system components include a variable speed hydraulically driven coolant pump and radiator fan, two servo-solenoid hydraulic control valves to operate the pump and fan hydraulic motors, and six immersion electrical heaters to heat the coolant. A thermostat valve was not inserted into the cooling loop so that this study might exclusively focus on the hydraulic operated water pump and radiator fan.

2.1. Automotive engine and radiator thermal dynamics

The cooling system's dynamic behavior may be represented by a reduced order two-node lumped parameter thermal model (refer to Fig. 1) to minimize the computational burden for possible in-vehicle implementation. The engine and radiator temperature dynamic behaviors (Salah, Mitchell, Wagner, & Dawson, 2008) may be expressed as

$$C_e\dot{T}_e = Q_{in} - c_{pc}\dot{m}_c(T_e - T_r), \tag{1}$$

$$C_r\dot{T}_r = -Q_o + c_{pc}\dot{m}_c(T_e - T_r) - \varepsilon c_{pa}\dot{m}_a(T_e - T_\infty). \tag{2}$$

The variables $Q_{in}(t)$ and $Q_o(t)$ represent the heat input generated during the combustion process and the radiator heat loss due to uncontrollable air flow, respectively.

2.2. Hydraulic-driven coolant pump and radiator fan dynamics

Two servo-solenoid hydraulic valves operated the pump and fan hydraulic gear motors (Merritt, 1967). The control voltage, $V(t)$, applied to the solenoid coil generated a mechanical force which displaced the internal spool to allow fluid flow. The solenoid current, $i(t)$, and force, $F_s(t)$, are governed by (Vaughan & Gamble, 1996)

$$\frac{\mathrm{d}i}{\mathrm{d}t} = \frac{1}{L}(V - iR), \quad F_s = \left(\frac{N_t^2 a\mu_o}{4l_g}\right)i^2. \tag{3}$$

The magnitude of the transient and steady-state forces on the valve spool can be described as

$$F_{tr}^{1,2} = [L_d C_d w\sqrt{2\rho(P_{SB} - P_{AT})}]\dot{x},$$
$$F_{ss}^{1,2} = [2C_d w\cos(\theta)(P_{SB} - P_{AT})]x, \tag{4}$$

where $P_{SB} = P_s$ or P_B, and $P_{AT} = P_A$ or P_T. The superscripts in Eq. (4) denote the left and right lands. The hydraulic valve's internal spool displacement may be expressed as

$$\ddot{x} = \frac{1}{m_s}[F_s + (F_{ss}^2 - F_{ss}^1) + (F_{tr}^2 - F_{tr}^1) - k_{val}x - b_{val}\dot{x}]. \tag{5}$$

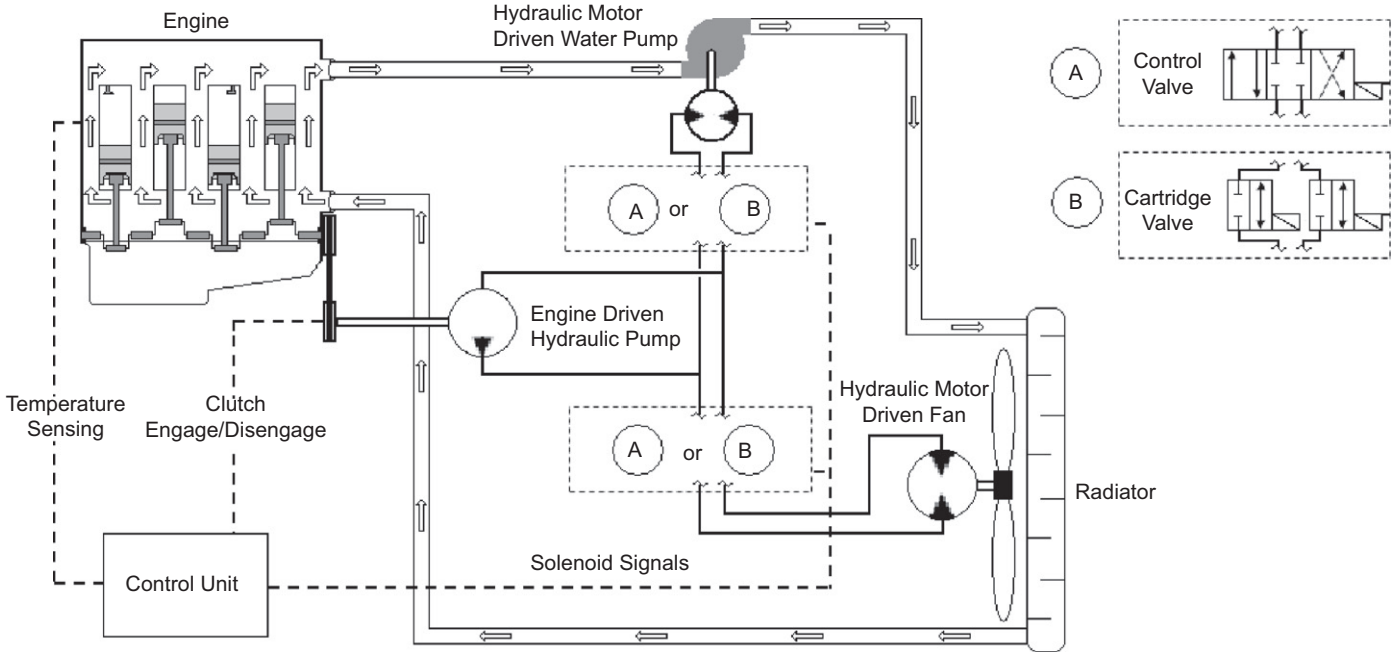

Fig. 1. Advance automotive cooling system featuring a variable speed hydraulic-driven coolant pump and radiator fan, control valves, and sensors (temperature, flow rate, pressure).

The valve's position, $x(t)$, determines the load flow, $Q_L(t)$, applied to the hydraulic motor and the corresponding load pressure, $P_L(t)$ (Merritt, 1967) such that

$$Q_L = D_m\omega + C_{im}P_L + \frac{V_t}{2\beta}\dot{P}_L = \left(C_d w\sqrt{\frac{(P_S - P_L)}{\rho}}\right)x, \tag{6}$$

$$\dot{P}_L = \left(\frac{2\beta C_d w}{V_t}\sqrt{\frac{(P_S - P_L)}{\rho}}\right)x - \frac{2\beta C_{im}}{V_t}P_L - \frac{2\beta D_m}{V_t}\omega. \tag{7}$$

The motor shaft acceleration, $\dot{\omega}(t)$, with an assumption of ideal power transformation is

$$\dot{\omega} = \frac{1}{J}(T_g - B_m\omega - T_L), \tag{8}$$

where $T_g \triangleq D_m P_L$ and $T_L \triangleq f_L(\dot{m})$. The variable $\dot{m}(t)$ denotes the mass flow rate of liquid or air. To facilitate the controller design process, an expression for $\omega(t)$ can be obtained from Eq. (7) and then substituted into Eq. (8) to realize

$$\dot{\omega} = \left(\frac{D_m^2 + B_m C_{im}}{JD_m}\right)P_L + \left(\frac{B_m V_t}{2JD_m\beta}\right)\dot{P}_L - \left(\frac{B_m}{JD_m}C_d w\sqrt{\frac{P_S - P_L}{\rho}}\right)x - \frac{T_L}{J}. \tag{9}$$

3. Hydraulic controller design

A Lyapunov-based nonlinear control algorithm has been developed to regulate the coolant temperature to a given set point and utilize hydraulic power in an efficient manner. The controller's main objective is to accurately track the temperature set point, $T_{ed}(t)$, while compensating for system uncertainties (i.e., combustion process heat input, $Q_{in}(t)$, radiator heat loss, $Q_o(t)$, pump hydraulic motor load, $T_{Lp}(t)$, fan hydraulic motor load, $T_{Lf}(t)$, hydraulic pump load pressure variations, $\dot{P}_{Lp}(t)$, and hydraulic fan load pressure variations, $\dot{P}_{Lf}(t)$ by harmoniously controlling the hydraulic actuators. Referring to Fig. 1, the system control components include two solenoid valves and two hydraulic-driven gear motors. For Eqs. (1), (2) and (9), the signals $T_e(t)$, $T_r(t)$ and $T_\infty(t)$ can be measured by either thermocouples or thermistors, the signal $\omega(t)$ can be measured by optical encoders, and system parameters B_m, c_{pa}, c_{pc}, C_d, C_e, C_{im}, C_r, D_m, J, V_t, w, β, ε and ρ are assumed to be known constants.

To facilitate the controller design process, four assumptions are imposed:

A1: The signals $Q_{in}(t)$ and $Q_o(t)$ always remain positive in Eqs. (1) and (2) (i.e., $Q_{in}(t)$, $Q_o(t) \geqslant 0$). Further, the signals $Q_{in}(t)$ and $Q_o(t)$ remain bounded at all time, such that $Q_{in}(t), Q_o(t) \in L_\infty$.

A2: The surrounding ambient temperature $T_\infty(t)$ is uniform and satisfies $T_e(t) - T_\infty(t) \geqslant \varepsilon_1$ at all time where ε_1 is a real positive constant.

A3: The heated coolant and radiator temperatures satisfy the condition $T_e(t) - T_r(t) \geqslant \varepsilon_2$ at all time where ε_2 is a real positive constant. Further, $T_e(0) \geqslant T_r(0)$ assists in the boundedness of signal argument.

A4: The signals $T_L(t)$, $P_L(t)$, and $P_S(t)$ always remain positive in Eq. (9) (i.e., $T_L(t), P_L(t), P_S(t) \geqslant 0$ at all time) and $P_S(t) > P_L(t)$. Further, the signals $T_L(t)$, $P_L(t)$, and its first time derivative, $\dot{P}_L(t)$, remain bounded at all time, such that $T_L(t), P_L(t), \dot{P}_L(t) \in L_\infty$.

Note that Assumption A3 allows the heated coolant and radiator to initially be at the same temperature (e.g., cold start); the unlikely case of $T_e(0) < T_r(0)$ has not been considered.

3.1. Backstepping robust control

The control objective is to ensure that the measured temperatures of the engine coolant, $T_e(t)$, and the radiator, $T_r(t)$, track the desired trajectories $T_{ed}(t)$ and $T_{vr}(t)$. Further, the measured pump speed, $\omega_p(t)$, and fan speed, $\omega_f(t)$, should track the desired trajectories $\omega_{pd}(t)$ and $\omega_{fd}(t)$. These four requirements can be expressed mathematically as

$$|T_{ed}(t) - T_e(t)| \leqslant \varepsilon_e, \quad |T_r(t) - T_{vr}(t)| \leqslant \varepsilon_r,$$
$$|\omega_{pd}(t) - \omega_p(t)| \leqslant \varepsilon_p, \quad |\omega_{fd}(t) - \omega_f(t)| \leqslant \varepsilon_f \quad \text{as } t \to \infty. \tag{10}$$

The controller must also compensate for the system variable uncertainties $Q_{in}(t)$, $Q_o(t)$, $\dot{P}_{Lp}(t)$, $\dot{P}_{Lf}(t)$, $T_{Lp}(t)$, and $T_{Lf}(t)$ where ε_e, ε_r, ε_p and ε_f are real positive constants.

Remark 1. Although it is unlikely that the desired radiator temperature setpoint, $T_{vr}(t)$, hydraulic coolant pump speed, $\omega_{pd}(t)$, and hydraulic radiator fan speed, $\omega_{fd}(t)$, are required (or known) by the automotive engineer, it will be shown that the radiator setpoint temperature, pump speed, and fan speed can be indirectly designed based on the engine's thermal conditions and commutation strategy (refer to Remark 2).

Two additional assumptions are imposed to assist in the controller design process:

A5: The engine temperature profile is always bounded and chosen such that its first time derivative remains bounded at all times (i.e., $T_{ed}(t), \dot{T}_{ed}(t) \in L_\infty$). Further, $T_{ed}(t) \gg T_\infty(t)$ at all times.

A6: The engine temperature profile and radiator temperature satisfy the condition $T_{ed}(t) - T_r(t) \geqslant \varepsilon_3$ at all time where ε_3 is a real positive constant. This assumption is needed to facilitate the boundedness argument in the controller development.

To quantify the temperature tracking objective, the tracking error signals $\eta_e(t)$, $\eta_r(t)$, $\eta_p(t)$, and $\eta_f(t)$ are defined as

$$\eta_e \triangleq T_{ed} - T_e, \quad \eta_r \triangleq T_r - T_{vr}, \quad \eta_p \triangleq \omega_{pd} - \omega_p,$$
$$\eta_f \triangleq \omega_{fd} - \omega_f. \tag{11}$$

By adding and subtracting $MT_{vr}(t)$ to Eq. (1), and expanding the variables $\dot{m}_c \triangleq \rho_c c_c \omega_p$, $\dot{m}_a \triangleq \rho_a c_a \omega_f$, $M \triangleq M_1\omega_{po}$, $M_1 \triangleq c_{pc}\rho_c c_c$, $M_2 \triangleq \varepsilon c_{pa}\rho_a c_a$, and $\omega_{pd} \triangleq \bar{\omega}_{pd} + \omega_{po}$, the engine and radiator dynamics of Eqs. (1) and (2) can be rewritten as

$$C_e\dot{T}_e = Q_{in} - M_1(\bar{\omega}_{pd} - \eta_p)(T_e - T_r) - M(T_e - T_{vr}) + M\eta_r, \tag{12}$$

$$C_r\dot{T}_r = -Q_o + M_1(\omega_{pd} - \eta_p)(T_e - T_r) - M_2(\omega_{fd} - \eta_f)(T_e - T_\infty), \tag{13}$$

where ω_{po} is a positive design constant that represent the minimum coolant pump speed, and c_c, c_a, ρ_c and ρ_a are real positive fully known constants. The dynamics of the coolant pump and radiator fan hydraulic motors can be rewritten using Eq. (9) as

$$\frac{J_p}{x_{mp}}\dot{\omega}_p = f_p - M_p X_p, \quad \frac{J_f}{x_{mf}}\dot{\omega}_f = f_f - M_f X_f, \tag{14}$$

where

$$f_p \triangleq \left(\frac{D_{mp}^2 + B_{mp}C_{imp}}{D_{mp}x_{mp}}\right)P_{Lp} + \left(\frac{B_{mp}V_{tp}}{2D_{mp}\beta_p x_{mp}}\right)\dot{P}_{Lp} - \frac{T_{Lp}}{x_{mp}},$$

$$M_p \triangleq \frac{B_{mp}}{D_{mp}}C_{dp}w_p\sqrt{\frac{P_{Sp} - P_{Lp}}{\rho_p}}, \quad X_p \triangleq \frac{x_p}{x_{mp}},$$

$$f_f \triangleq \left(\frac{D_{mf}^2 + B_{mf}C_{imf}}{D_{mf}x_{mf}}\right)P_{Lf} + \left(\frac{B_{mf}V_{tf}}{2D_{mf}\beta_f x_{mf}}\right)\dot{P}_{Lf} - \frac{T_{Lf}}{x_{mf}},$$

$$M_f \triangleq \frac{B_{mf}}{D_{mf}}C_{df}w_f\sqrt{\frac{P_{Sf}-P_{Lf}}{\rho_f}},$$

and $X_f \triangleq x_f/x_{mf}$.

3.2. Closed-loop error system development and controller formulation

The open-loop error system can be analyzed by taking the first time derivative of all the expressions in Eq. (11) and then multiplying both sides of the resulting equations by C_e, C_r, J_p/x_{mp}, and J_f/x_{mf} for the engine, radiator, hydraulic coolant pump, and hydraulic radiator fan dynamics, respectively. The system dynamics in Eqs. (12)–(14) can be substituted in the resulting equations and then reformatted to realize

$$C_e\dot{\eta}_e = C_e\dot{T}_{ed} - Q_{in} + M(T_e - T_{vro}) - M\eta_r - M_1(T_e - T_r)\eta_p - u_e, \tag{15}$$

$$C_r\dot{\eta}_r = -Q_o + M(T_e - T_r) - M_1(T_e - T_r)\eta_p + M_2(T_e - T_\infty)\eta_f - C_r\dot{T}_{vr} + u_r, \tag{16}$$

$$\frac{J_p}{x_{mp}}\dot{\eta}_p = \frac{J_p}{x_{mp}}\dot{\omega}_{pd} - f_p + u_p, \quad \frac{J_f}{x_{mf}}\dot{\eta}_f = \frac{J_f}{x_{mf}}\dot{\omega}_{fd} - f_f + u_f. \tag{17}$$

In these expressions, Eq. (9) was utilized plus $T_{vr} \triangleq \bar{T}_{vr} + T_{vro}$, $u_e \triangleq M\bar{T}_{vr} - M_1(T_e - T_r)\bar{\omega}_{pd}$, $u_r \triangleq M_1(T_e - T_r)\bar{\omega}_{pd} - M_2(T_e - T_\infty)\omega_{fd}$, $u_p \triangleq M_pX_p$, and $u_f \triangleq M_fX_f$. The parameter T_{vro} is a positive design constant.

Remark 2. The control inputs $\bar{T}_{vr}(t)$, $\bar{\omega}_{pd}(t)$, $\omega_{fd}(t)$, $X_p(t)$, and $X_f(t)$ are uni-polar. Hence, commutation strategies are designed utilizing the bi-polar control laws $u_e(t)$, $u_r(t)$, $u_p(t)$ and $u_f(t)$ as

$$\bar{\omega}_{pd} \triangleq \frac{[\mathrm{sgn}(u_e)-1]u_e}{2M_1(T_e - T_r)}, \quad \bar{T}_{vr} \triangleq \frac{[1+\mathrm{sgn}(u_e)]u_e}{2M}, \quad \omega_{fd} \triangleq \frac{[1+\mathrm{sgn}(F)]F}{2M_2(T_e - T_\infty)}, \tag{18}$$

$$X_p \triangleq \frac{[1+\mathrm{sgn}(u_p)]u_p}{2M_p}, \quad X_f \triangleq \frac{[1+\mathrm{sgn}(u_f)]u_f}{2M_f}, \tag{19}$$

where M_1, M_2, M_p and M_f were introduced in Eqs. (12)–(14), and $F \triangleq M_1(T_e - T_r)\bar{\omega}_{pd} - u_r$. The control input, $\omega_{fd}(t)$ is obtained from Eq. (18) after $\bar{\omega}_{pd}(t)$ is computed. From these definitions, if $u_e(t), u_r(t), u_p(t), u_f(t) \in L_\infty$ at all time, then $\bar{\omega}_{pd}(t), \bar{T}_{vr}(t)$, $\omega_f(t), X_p(t), X_f(t) \in L_\infty$ at all time. The commutation strategies presented in Eqs. (18) and (19) are developed in a similar manner to those presented in Salah et al. (2008).

The expressions in Eqs. (15)–(17) may be rewritten as

$$C_e\dot{\eta}_e = N_e - M\eta_r - M_1(T_e - T_r)\eta_p - u_e, \tag{20}$$

$$C_r\dot{\eta}_r = N_r - M_1(T_e - T_r)\eta_p + M_2(T_e - T_\infty)\eta_f - C_r\dot{T}_{vr} + u_r, \tag{21}$$

$$\frac{J_p}{x_{mp}}\dot{\eta}_p = N_p + \frac{J_p}{x_{mp}}\dot{\omega}_{pd} + u_p, \quad \frac{J_f}{x_{mf}}\dot{\eta}_f = N_f + \frac{J_f}{x_{mf}}\dot{\omega}_{fd} + u_f, \tag{22}$$

where the functions $N_e(T_e, t)$, $N_r(T_e, T_r, t)$, $N_p(P_{Lp}, \dot{P}_{Lp}, T_{Lp}, t)$, and $N_f(P_{Lf}, \dot{P}_{Lf}, T_{Lf}, t)$ are defined as

$$N_e \triangleq C_e\dot{T}_{ed} - Q_{in} + M(T_e - T_{vro}), \quad N_r \triangleq M(T_e - T_r) - Q_o, \quad N_p \triangleq -f_p, \quad N_f \triangleq -f_f. \tag{23}$$

These functions can be upper bounded as $N_e \leqslant \varepsilon_{ee}$, $N_r \leqslant \varepsilon_{rr}$, $N_p \leqslant \varepsilon_{pp}$, and $N_f \leqslant \varepsilon_{ff}$ based on Assumptions A1, A3–A5, and A7, where ε_{ee}, ε_{rr}, ε_{pp} and ε_f are positive constants. By utilizing a Lyapunov stability analysis, the control laws $u_e(t)$, $u_r(t)$, $u_p(t)$ and $u_f(t)$, introduced in Eqs. (15)–(17), are designed as shown in Table 1.

For Table 1, the variable $F(t)$ was introduced in Eq. (18), K_e is a positive control gain, and the variables $B_1(\bullet)$ through $B_{49}(\bullet)$ are defined in Appendix A. The knowledge of $u_e(t)$, $u_r(t)$, $u_p(t)$ and $u_f(t)$, based on Table 1, allows the commutation relationships of Eqs. (18) and (19) to be calculated which provides $\bar{T}_{vr}(t)$, $\bar{\omega}_{pd}(t)$, $\omega_{fd}(t)$, $X_p(t)$, and $X_f(t)$. Finally, the voltage signals for the pump and fan servo-solenoid valves are prescribed using $X_p(t)$ and $X_f(t)$ with *a priori* empirical relationships.

3.3. Stability analysis

A Lyapunov stability analysis guarantees that the advanced thermal management system will be stable when applying the control laws introduced in Table 1.

Theorem 1. *The controller given in Table 1 ensures that*: (i) *all closed-loop signals stay bounded for all time*; *and* (ii) *tracking is uniformly ultimately bounded* (*UUB*) *in the sense that* $|\eta_e(t)| \leqslant \varepsilon_e$, $|\eta_r(t)| \leqslant \varepsilon_r$, $|\eta_p(t)| \leqslant \varepsilon_p$, $|\eta_f(t)| \leqslant \varepsilon_f$ *as* $t \to \infty$.

Proof. See Appendix B for the complete Lyapunov stability analysis.

Table 1
The control laws $u_e(t)$, $u_r(t)$, $u_p(t)$, and $u_f(t)$ for the hydraulic actuators.

Case	Condition	u_e	u_r	u_p	u_f
I	$u_e > 0,\ F \leqslant 0$	$K_e\eta_e$	$B_1\eta_e + B_2\eta_r$	$B_9\eta_e + B_{10}\eta_r + B_{11}\eta_p$	$B_{27}\eta_r + B_{28}\eta_f$
II	$u_e \leqslant 0,\ F \leqslant 0$		$B_3\eta_e + B_4\eta_r$	$B_{12}\eta_e + B_{13}\eta_r + B_{14}\eta_p + B_{15}\eta_e\eta_r + B_{16}\eta_e\eta_p + B_{17}\eta_e^2$	$B_{29}\eta_r + B_{30}\eta_f + B_{31}\eta_e\eta_p$
III	$u_e > 0,\ F > 0$		$B_5\eta_e + B_6\eta_r$	$B_{18}\eta_e + B_{19}\eta_r + B_{20}\eta_p$	$B_{32}\eta_e + B_{33}\eta_r + B_{34}\eta_p + B_{35}\eta_f + B_{36}\eta_e\eta_r + B_{37}\eta_e\eta_p + B_{38}\eta_r\eta_p + B_{39}\eta_e^2 + B_{40}\eta_r^2$
IV	$u_e \leqslant 0,\ F > 0$		$B_7\eta_e + B_8\eta_r$	$B_{21}\eta_e + B_{22}\eta_r + B_{23}\eta_p + B_{24}\eta_e\eta_r + B_{25}\eta_e\eta_p + B_{26}\eta_e^2$	$B_{41}\eta_e + B_{42}\eta_r + B_{43}\eta_p + B_{44}\eta_f + B_{45}\eta_e\eta_r + B_{46}\eta_e\eta_p + B_{47}\eta_r\eta_p + B_{48}\eta_e^2 + B_{49}\eta_r^2$

4. Experimental test bench

An experimental test bench (refer to Fig. 2) has been assembled to validate the advanced thermal management system controller design in a flexible, repeatable, and safe testing environment. The test bench featured six immersion heaters, a hydraulic-driven coolant pump, hydraulic actuated radiator fan, two hydraulic servo control valves, and various sensors. Six Temco (TSPO 2084) immersion coils heated coolant (12 kW) that circulated within the system. Note that the limited fluid heating capabilities of the six coils necessitated the selection of lower set point temperatures in Section 5. Once heated, the fluid was circulated via a hydraulically driven centrifugal pedestal mount coolant pump (e.g., maximum 220LPM) through a radiator (6.8L capacity) where forced convection (e.g., maximum 42 m^3/min) was provided by a hydraulically driven fan. The pump and radiator fan were driven by Haldex hydraulic motors with maximum displacements of 6.36 and 11.65 cm^3/rev, respectively. The hydraulic flow to the motors was controlled with either two servo-solenoid proportional control valves (BOSCH NG 6) and accompanying Bosch PL 6 amplifier cards, or four solenoid operated cartridge/poppet valves (Parker B09-2-6P). The supply pressure for the hydraulic components was provided by a 5.6 kW Baldor industrial electric motor spinning a Bosch hydraulic pump with a displacement of 16.39 cm^3/rev.

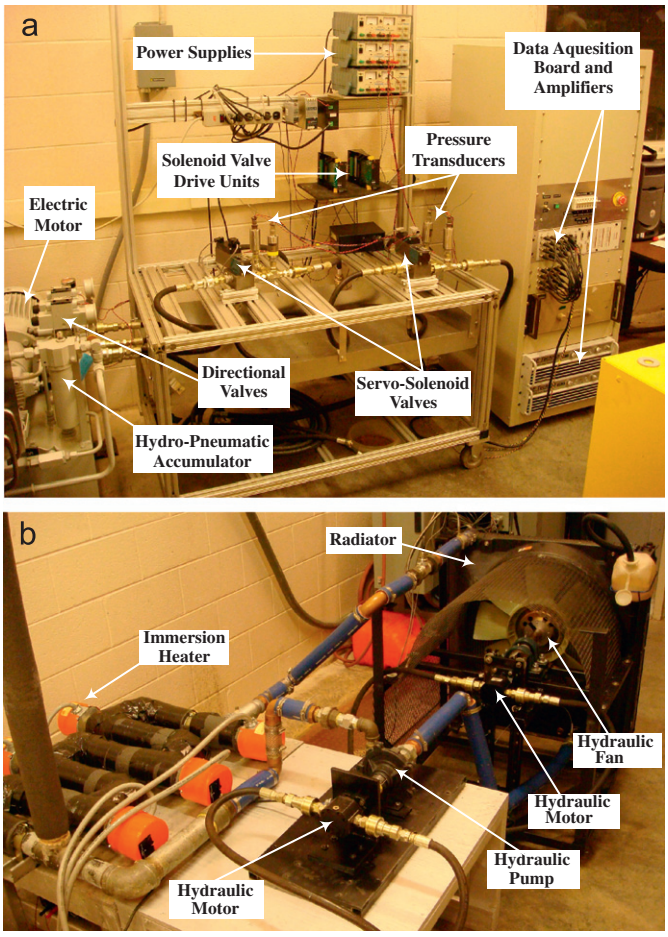

Fig. 2. Experimental hydraulic-based automotive thermal test bench: (a) hydraulic system that features an electric motor, accumulator, two directional valves, two servo-solenoid proportional control valves, solenoid valve drive units, and pressure transducers and (b) thermal system with six immersion heating coils, hydraulic-driven coolant pump, radiator with a hydraulic-driven fan, and various (e.g., temperature, flow rate, and motor speed) sensors.

The engine (radiator inlet) and radiator outlet temperatures were measured using two K-type thermocouples, while the ambient temperature was measured by a single J-type thermocouple. All thermocouple signals were isolated, amplified, and linearized via OMEGA OM5 signal conditioners. Two Monarch Instruments optical sensors (ROS-W 6180-056) measured the actuators' rotational speed, while a turbine flow meter (TR-1000) recorded the coolant flow rate. Honeywell (Sensotec) A-5 pressure transducers measured the hydraulic supply and return pressures. Data acquisition and control was accomplished with a dSPACE 1104 board.

The controller board interfaced with Matlab/Simulink allowing for real-time execution of the control strategies. The coding in Simulink permitted flexibility to implement C code, Matlab M-files, and Simulink block diagrams. In addition, dSPACE's "Control Desk" software monitored the experiments and permitted the capture of experimental results. The controller dynamics were described in Matlab/Simulink and executed in real time. The capabilities of the hardware and the slower dynamics of automotive cooling systems allow the detailed controller design to be implemented without concerns in the laboratory.

5. Numerical and experimental results

In this section, simulation and experimental results will be presented to demonstrate the backstepping controller's ability to

Table 2
Numerical and experimental model parameter and backstepping controller values.

Symbol	Value	Unit	Symbol	Value	Unit	Symbol	Value	Unit
B_{mp}	9.50e−01	N s/cm	K_e	1.50e+03[a]	–	w_p	3.62[a]	cm^2/cm
B_{mf}	5.31	N s/cm	K_f	2.50e+03[a]	–	W_f	3.62[a]	cm^2/cm
c_{pa}	1.01[a]	kJ/kg K	K_p	2.00e+03[a]	–	x_{mp}	3.00[a]	mm
c_{pc}	4.18[a]	kJ/kg K	K_r	1.50e+03[a]	–	x_{mf}	3.00[a]	mm
C_{dp}	6.30e−01[a]	–	M_1	4.18[a]	kJ/m^3 K	β_p	6.89e+02	MPa
C_{df}	6.30e−01[a]	–	M_2	6.33e−01[a]	kJ/m^3 K	β_f	6.89e+02	MPa
C_e	3.30e−01[a]	kJ/K	P_{Sp}	3.45e+03[a]	kPa	ε	6.30e−03[a]	–
C_{imp}	2.50e−03	cm^5/N s	P_{Sf}	6.89e+03[a]	kPa	ρ_a	1.18[a]	kg/m^3
C_{imf}	2.50e−03	cm^5/N s	T_{Lp}	3.00e+01	N m	ρ_c	9.97e+02[a]	kg/m^3
C_r	2.50e−01[a]	kJ/K	T_{Lf}	6.00e+01	N m	ρ_f	9.00e+02[a]	kg/m^3
D_{mp}	1.01[a]	cm^3/rad	T_{vro}	3.17e+02[a]	K	ρ_p	9.00e+02[a]	kg/m^3
D_{mf}	1.85[a]	cm^3/rad	T_∞	3.00e+02[a]	K	ω_{po-SIM}	3.50e+01[a]	rad/s
J_p	9.04e−01	kg cm^2	V_{tp}	1.19e+05	cm^3	ω_{po-EXP}	4.00e+01[a]	rad/s
J_f	1.13	kg cm^2	V_{tf}	3.68e+04	cm^3			

[a] For real-time implementation of the proposed controller, the 32 required parameters are denoted by the superscript.

track temperature setpoints. First, A Matlab/Simulink™ simulation has been created to evaluate and analyze the robustness of the nonlinear control algorithm to noise and prescribed loads. Next, two experimental scenarios (e.g., variable heat with ram air, steady heat) have been investigated to emulate typical ground vehicle operating profiles. The system model parameters and controller values are summarized in Table 2. Note that the value of minimum coolant pump speed, ω_{po}, for the simulation differs from its value in the experiment as shown in Table 2. Setting the magnitude at the same value does not change the experimental results; however, the coolant pump must operate experimentally above a certain threshold which may impact the power consumption in the long run.

5.1. Numerical results

A numerical simulation of the backstepping robust control strategy listed in Table 1 has been performed on the system dynamics in Eqs. (12)–(14). For added reality, band-limited white noise was added to the sensors' measurement (e.g., noise power = 10^{-5}, sampling time = 5.0e−03 s). A series of constant mechanical loads, T_{Lp} and T_{Lf}, were applied to the hydraulic coolant pump and radiator fan. A "load" cycle (e.g., $10 \leqslant Q_{in} \leqslant 24$ kW) and external ram air disturbance (e.g., $0 \leqslant Q_o \leqslant 15$ kW) were introduced as shown in Fig. 3a and b. The desired engine temperature was $T_{ed} = 322$ K. The initial simulation conditions were $T_e(0) = 313.7$ K and $T_r(0) = \ = 310.9$ K.

In Fig. 3c and d, the response of the engine and radiator temperatures and the engine temperature tracking error have been presented for the variable heat input and ram air disturbance. The engine temperature was regulated to $|\eta_{ess}| \leqslant 0.5$ K despite the heat and external air variations. The radiator temperature spiked at approximately $t = 1000$ and 1700 s when the heat input, $Q_{in}(t)$, significantly decreased. The speed of the hydraulic coolant pump and radiator fan are displayed in Fig. 3e and f. The hydraulic pump speed seeks its maximum value, $\omega_p = 150$ rad/s, due to the heat increase at $t = 300$ s. Note that the coolant pump effort increased as the fan effort decreased which is ideal for power minimization.

5.2. Experimental testing

Several comprehensive tests have been conducted on the hydraulic-based thermal test bench to investigate the robust controller design performance and compare it against several classical controllers. The initial test scenario varied both the heat input and air disturbance. Specifically, $Q_{in}(t)$ changes from 8 to 12 kW while $Q_o(t)$ has been selected such that it emulates a vehicle traveling at 35 km/h $t = 3000$ s. In Fig. 4a, the engine and radiator temperature responses are presented for the sinusoidal setpoint $T_{ed} = 322 + 2\sin(\pi t/150)$ K. The nonlinear controller accommodated the heat input and ram air variations satisfactory in Fig. 4b with the peak engine temperature absolute value steady-state tracking error of $|\eta_{ep}| \leqslant 0.9$ K. The hydraulic coolant pump and radiator fan speeds are displayed in Fig. 4c and d. The coolant pump speed remains relatively steady with the heat variations, but the radiator fan introduces 10% more effort to reject the system heat for $1500 < t < 3000$ s.

The next case applies a fixed heat input of $Q_{in} = 12$ kW (i.e., six heaters) and no ram air disturbance (i.e., parked vehicle). For this test, the desired temperature profile was selected to be a sinusoidal with $T_{ed} = 322 + 2\sin(\pi t/150)$ K. In Fig. 5a, the engine and radiator temperature responses have been presented which demonstrate that the actual engine temperature successfully tracked the desired temperature profile. In Fig. 5b, the controller achieved a steady-state absolute value temperature tracking error of $|\eta_{ess}| \leqslant 0.7$ K. In Fig. 5c and d, the hydraulic coolant pump and radiator fan responses have been presented with a combined power consumption of $P_{sys} = 165.2$ W.

Table 3 summarizes the second experimental test results for the backstepping robust controller, as well as two other controllers (e.g., PID, PWM) for comparison purposes. The initial conditions and temperature set points were maintained for the three controller designs. The backstepping robust controller (Case 1) achieved the smallest absolute steady-state engine temperature tracking error, $|\eta_{ess}| = 0.7$ K, when compared to the PID and PWM (poppet valve) controllers. For Case 3, the PWM control effort essentially operated in a bang/bang manner at $f = 1$ Hz which reduced power consumption (refer to Remark 3) by 23% to $P_{sys} = 127.9$ W when compared to Case 1. The focus of the comparisons in Table 3 were primarily temperature tracking error and power consumption since they have been deemed critical in this study. Overall, the backstepping robust controller demonstrated the best temperature tracking error but consumed the most power. The proposed controller offers greater precision in tracking desired temperatures and rejecting disturbances per Fig. 4 when compared with the other techniques. However, the controller derivation was rather complex when compared to the classical PID controller (Case 2). Note that the PID controller offered satisfactory performance as evident by a 2.8% reduction in power while increasing the temperature tracking error by 71.4% when comparing the absolute and steady-state errors, $|\eta_{ess}| = 1.2$ K verses $|\eta_{ess}| = 0.7$ K, for the backstepping robust controller. Finally, the PWM controller's operation was not practical given the bang/bang nature of the fan's operation and maintenance concerns.

Remark 3. The power measure

$$P_{sys} = \frac{1}{T}\int_{t_0}^{t} [P_{Lp}(\tau)Q_{Lp}(\tau) + P_{Lf}(\tau)Q_{Lf}(\tau)]\,\mathrm{d}\tau$$

calculates the average power consumed by the system actuators during the test period.

6. Summary

An advanced vehicle thermal management system can track engine temperature profiles while regulating cooling component power consumption. In this paper, hydraulic-based cooling system components have been mathematically modeled, simulated, experimentally assembled, and controlled utilizing a Lyapunov-based nonlinear backstepping controller. The proposed controller successfully maintained the coolant temperature to its setpoint with an improvement in the steady-state tracking error when compared to classical controllers. More importantly, the project demonstrated that hydraulic thermal management can be accomplished with harmonious pump and fan control. An excellent opportunity exists to integrate hydraulic actuated engine cooling system components into ground vehicles for active temperature regulation.

Appendix A. Control parameter definitions

The control parameters in Table 1 are bounded from Assumptions A2, A3, and A6 and may be described as

$$B_1 \triangleq M - \frac{K_e^2 C_r}{MC_e}, \quad B_2 \triangleq -\frac{K_e C_r}{C_e} - K_r, \quad B_3 \triangleq M, \quad B_4 \triangleq -K_r,$$

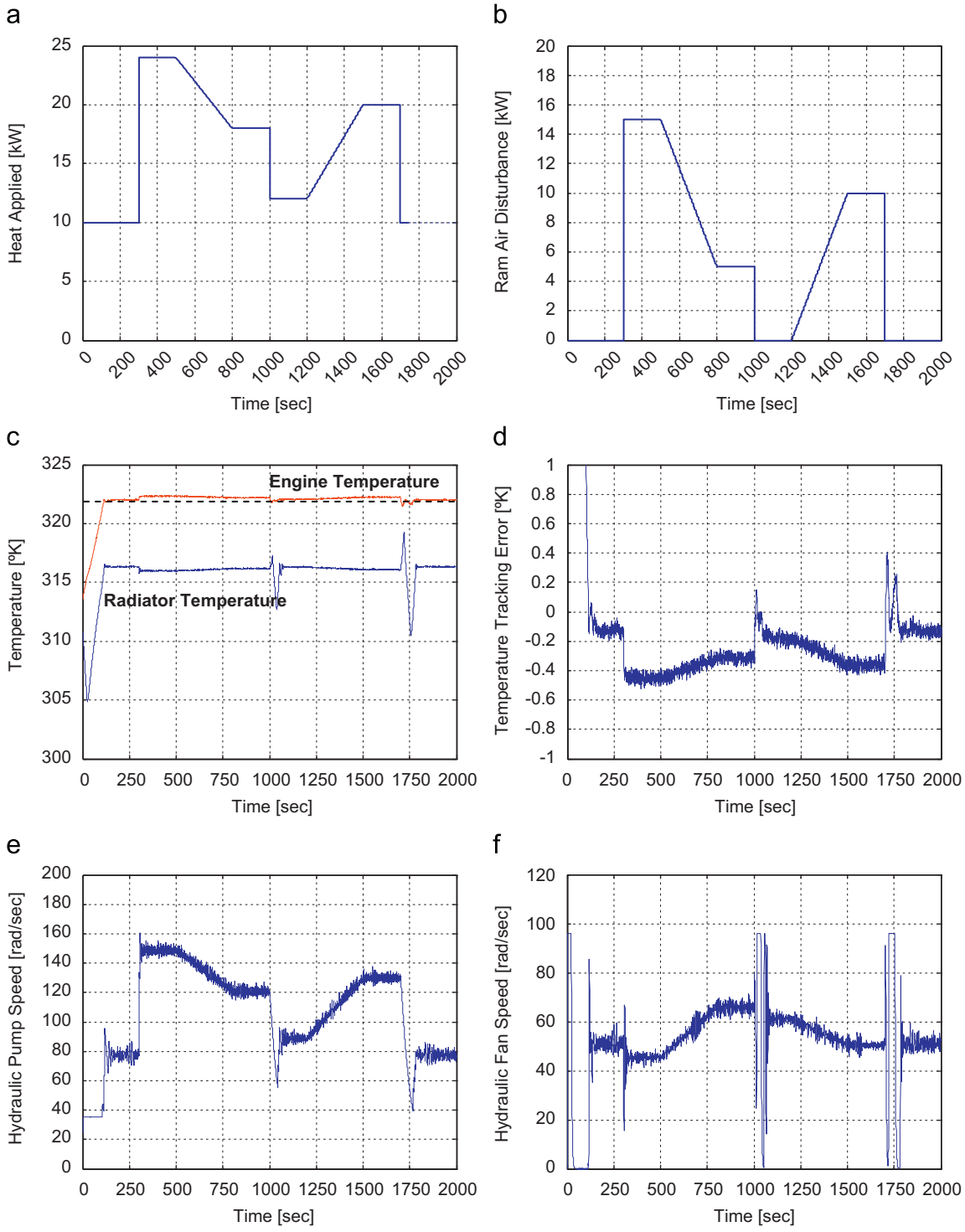

Fig. 3. Numerical response for variable engine thermal loads and ram air disturbance with: (a) heat input profile; (b) ram air disturbance, to emulate different vehicle speeds; (c) simulated engine and radiator temperatures response for a desired engine temperature of $T_{ed} = 322$ K; (d) simulated engine commanded temperature tracking error; (e) simulated coolant pump speed; and (f) simulated radiator fan speed.

$$B_5 \triangleq M - \frac{K_e^2 C_r}{MC_e}, \quad B_6 \triangleq -\frac{K_e C_r}{C_e} - K_r, \quad B_7 \triangleq M, \quad B_8 \triangleq -K_r,$$

$$B_9 \triangleq M_1(T_e - T_r), \quad B_{10} \triangleq M_1(T_e - T_r)\left[1 - \frac{K_e C_r}{MC_e}\right],$$

$$B_{11} \triangleq -K_p,$$

$$B_{12} \triangleq M_1(T_e - T_r) + \frac{J_p K_e M}{M_1 C_r x_{mp}(T_e - T_r)} + \frac{J_p K_e^2 (T_r - T_{ed})}{M_1 C_e x_{mp}(T_e - T_r)^2},$$

$$B_{13} \triangleq M_1(T_e - T_r) + \frac{J_p K_e M(T_r - T_{ed})}{M_1 C_e x_{mp}(T_e - T_r)^2},$$

$$B_{14} \triangleq \frac{J_p K_e (T_r - T_{ed})}{C_e x_{mp}(T_e - T_r)} - K_p, \quad B_{15} \triangleq -\frac{J_p K_e K_r}{M_1 C_r x_{mp}(T_e - T_r)^2},$$

$$B_{16} \triangleq -\frac{J_p K_e}{C_r x_{mp}(T_e - T_r)}, \quad B_{17} \triangleq \frac{J_p K_e M}{M_1 C_r x_{mp}(T_e - T_r)^2},$$

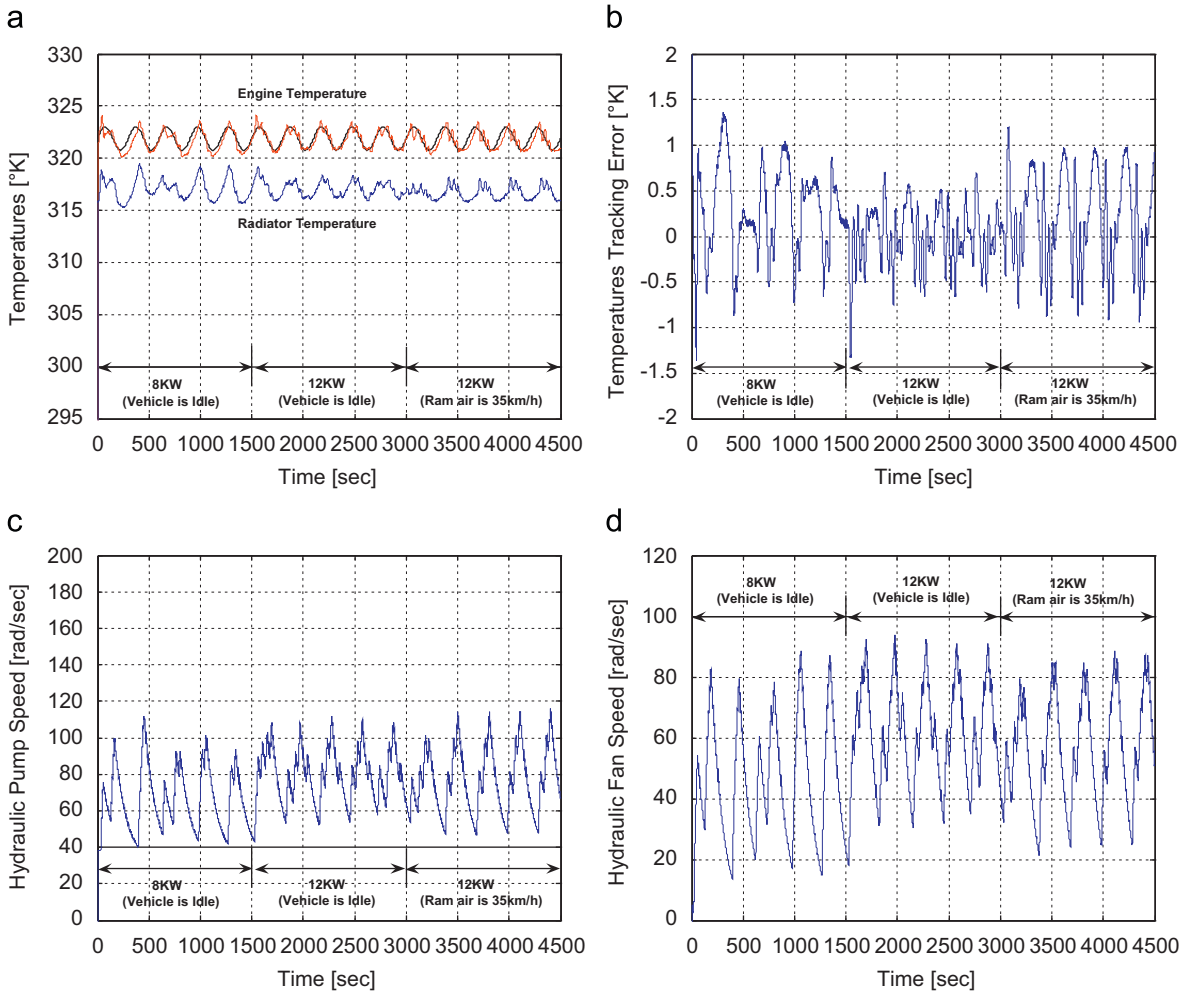

Fig. 4. First experimental test with a variable heat input and ram air disturbance for (a) experimental engine and radiator temperatures with $T_{ed} = 322 + 2\sin(\pi t/150)$ K; (b) experimental engine temperature tracking error; (c) experimental coolant mass flow rate through the pump; and (d) experimental air mass flow rate through the radiator fan.

$$B_{18} \triangleq M_1(T_e - T_r), \quad B_{19} \triangleq M_1(T_e - T_r)\left[1 - \frac{K_e C_r}{MC_e}\right],$$

$$B_{20} \triangleq -K_p,$$

$$B_{21} \triangleq M_1(T_e - T_r) + \frac{J_p K_e M}{M_1 C_r x_{mp}(T_e - T_r)} + \frac{J_p K_e^2 (T_r - T_{ed})}{M_1 C_e x_{mp}(T_e - T_r)^2},$$

$$B_{22} \triangleq M_1(T_e - T_r) + \frac{J_p K_e M(T_r - T_{ed})}{M_1 C_e x_{mp}(T_e - T_r)^2},$$

$$B_{23} \triangleq -K_p + \frac{J_p K_e (T_r - T_{ed})}{C_e x_{mp}(T_e - T_r)}, \quad B_{24} \triangleq -\frac{J_p K_e K_r}{M_1 C_r x_{mp}(T_e - T_r)^2},$$

$$B_{25} \triangleq -\frac{J_p K_e}{C_r x_{mp}(T_e - T_r)}, \quad B_{26} \triangleq \frac{J_p K_e M}{M_1 C_r x_{mp}(T_e - T_r)^2},$$

$$B_{27} \triangleq -M_2(T_e - T_\infty), \quad B_{28} \triangleq -K_f, \quad B_{29} \triangleq -M_2(T_e - T_\infty),$$

$$B_{30} \triangleq -K_f, \quad B_{31} \triangleq \frac{J_p K_e M_2 (T_e - T_\infty)}{M_1 C_r x_{mp}(T_e - T_r)^2},$$

$$B_{32} \triangleq \frac{-2J_f K_e M}{M_2 C_e x_{mf}(T_e - T_\infty)} + \frac{J_f K_e^3 C_r}{M_2 M C_e^2 x_{mf}(T_e - T_\infty)} - \frac{J_f K_r M}{M_2 C_r x_{mf}(T_e - T_\infty)} + \frac{J_f M^2 (T_e - T_{vro})}{M_2 C_e x_{mf}(T_e - T_\infty)^2} - \frac{J_f K_e^2 C_r (T_e - T_{vro})}{M_2 C_e^2 x_{mf}(T_e - T_\infty)^2},$$

$$B_{33} \triangleq \frac{J_f K_e^2 C_r}{M_2 C_e^2 x_{mf}(T_e - T_\infty)} + \frac{J_f K_e K_r}{M_2 C_e x_{mf}(T_e - T_\infty)} + \frac{J_f K_r^2}{M_2 C_r x_{mf}(T_e - T_\infty)} - \frac{J_f K_e M C_r (T_e - T_{vro})}{M_2 C_e^2 x_{mf}(T_e - T_\infty)^2} - \frac{J_f K_r M (T_e - T_{vro})}{M_2 C_e x_{mf}(T_e - T_\infty)^2} - \frac{J_f M^2}{M_2 C_e x_{mf}(T_e - T_\infty)} - M_2(T_e - T_\infty),$$

$$B_{34} \triangleq \frac{J_f K_e M_1 (T_e - T_r)}{M_2 C_e x_{mf}(T_e - T_\infty)} + \frac{J_f K_r M_1 (T_e - T_r)}{M_2 C_r x_{mf}(T_e - T_\infty)} - \frac{J_f M_1 M (T_e - T_r)}{M_2 C_e x_{mf}(T_e - T_\infty)} - \frac{J_f K_e K_r M_1 (T_e - T_r)}{M_2 M C_e x_{mf}(T_e - T_\infty)},$$

$$B_{35} \triangleq -\frac{J_f K_e}{C_e x_{mf}} - \frac{J_f K_r}{C_r x_{mf}} - K_f,$$

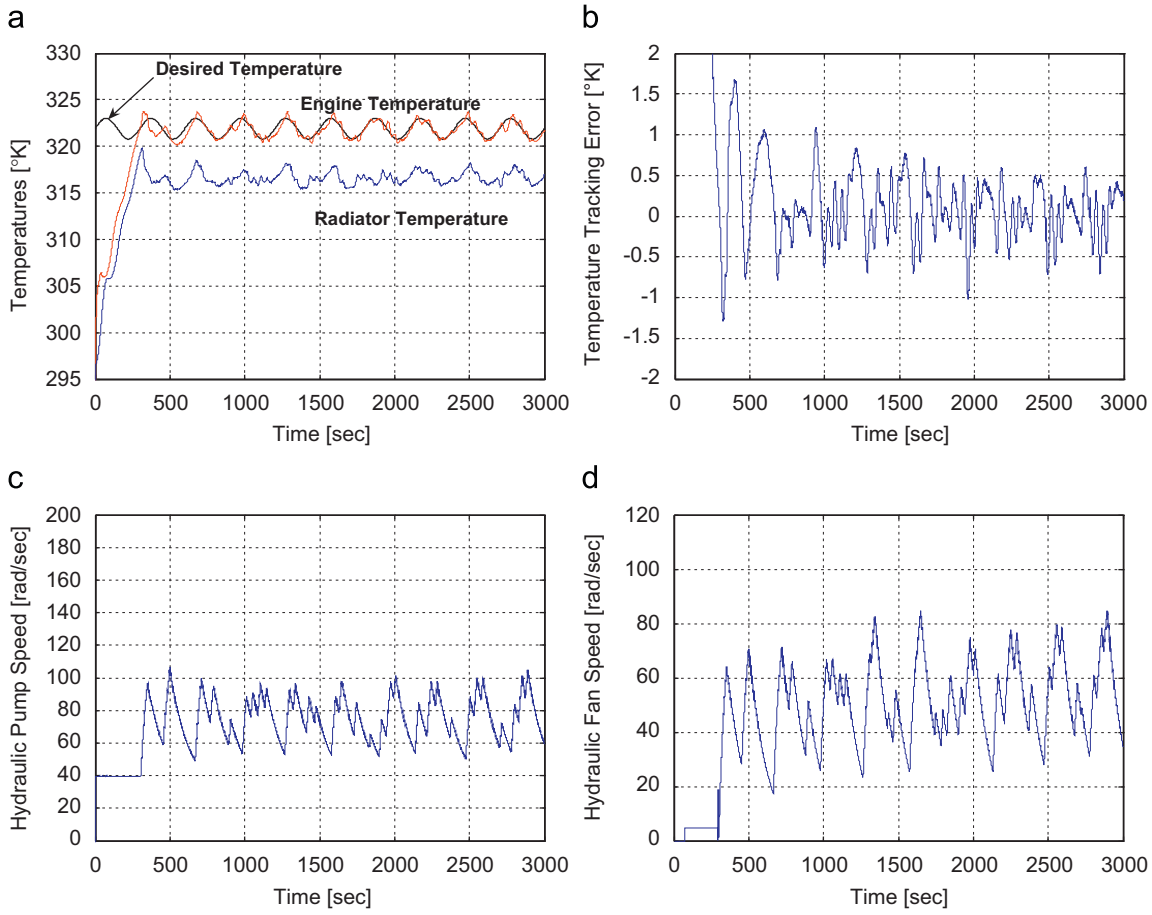

Fig. 5. Second experimental test with a constant heat input of $Q_{in} = 12$ kW and no ram air disturbance: (a) experimental engine and radiator temperatures with a desired sinusoidal engine temperature profile of $T_{ed} = 322 + 2\sin(\pi t/150)$ K; (b) experimental engine temperature tracking error; (c) experimental pump speed; and (d) experimental radiator fan speed.

Table 3
Experimental summary for three cooling system control strategies with steady heat, no ram air disturbance, and sinusoidal temperature tracking (test two).

Case	Operation strategies description	Valve	$\lvert\eta_{ess}\rvert$ (K)	P_{sys} (W)
1	Backstepping robust controller	Servo-solenoid	0.7	165.2
2	PID controller	Servo-solenoid	1.2	160.5
3	PWM control method	Poppet	2.2	127.9

For Case 2, the PID controller's gains were $K_P = 0.26$, $K_I = 0.01$ and $K_D = 0.44$. For Case 3, the coolant pump speed was constant at 62.8 rad/s and the radiator fan was controlled by a PWM control method. The PWM frequency was $f = 1$ Hz with variable duty cycle and PID controller with $K_P = 0.02$, $K_I = 7.6\text{e}{-04}$, and $K_D = 0.04$.

$$B_{36} \triangleq -\frac{J_f M^2}{M_2 C_e x_{mf}(T_e - T_\infty)^2} + \frac{2J_f K_e^2 C_r}{M_2 C_e^2 x_{mf}(T_e - T_\infty)^2} + \frac{J_f K_e K_r}{M_2 C_e x_{mf}(T_e - T_\infty)^2},$$

$$B_{37} \triangleq -\frac{J_f M_1 M(T_e - T_r)}{M_2 C_e x_{mf}(T_e - T_\infty)^2} + \frac{J_f K_e^2 M_1 C_r(T_e - T_r)}{M_2 M C_e^2 x_{mf}(T_e - T_\infty)^2},$$

$$B_{38} \triangleq \frac{J_f K_e M_1 C_r(T_e - T_r)}{M_2 C_e^2 x_{mf}(T_e - T_\infty)^2} + \frac{J_f K_r M_1(T_e - T_r)}{M_2 C_e x_{mf}(T_e - T_\infty)^2},$$

$$B_{39} \triangleq -\frac{J_f K_e M}{M_2 C_e x_{mf}(T_e - T_\infty)^2} + \frac{J_f K_e^3 C_r}{M_2 M C_e^2 x_{mf}(T_e - T_\infty)^2},$$

$$B_{40} \triangleq \frac{J_f C_r K_e M}{M_2 C_e^2 x_{mf}(T_e - T_\infty)^2} + \frac{J_f K_r M}{M_2 C_e x_{mf}(T_e - T_\infty)^2},$$

$$B_{41} \triangleq -\frac{J_f K_e M(T_e - T_{vro})(T_r - T_\infty)}{M_2 C_e x_{mf}(T_e - T_r)(T_e - T_\infty)^2} + \frac{J_f M^2(T_e - T_{vro})}{M_2 C_e x_{mf}(T_e - T_\infty)^2} + \frac{J_f K_e^2(T_r - T_{ed})}{M_2 C_e x_{mf}(T_e - T_r)(T_e - T_\infty)} - \frac{J_f K_e M}{M_2 C_e x_{mf}(T_e - T_\infty)} - \frac{J_f K_r M}{M_2 C_r x_{mf}(T_e - T_\infty)},$$

$$B_{42} \triangleq -M_2(T_e - T_\infty) - \frac{J_f K_r M(T_e - T_{vro})}{M_2 C_e x_{mf}(T_e - T_\infty)^2} + \frac{J_f K_e M(T_r - T_{ed})}{M_2 C_e x_{mf}(T_e - T_r)(T_e - T_\infty)} - \frac{J_f M^2}{M_2 C_e x_{mf}(T_e - T_\infty)} + \frac{J_f K_r^2}{M_2 C_r x_{mf}(T_e - T_\infty)},$$

$$B_{43} \triangleq \frac{J_f K_e M_1(T_r - T_{ed})}{M_2 C_e x_{mf}(T_e - T_\infty)} - \frac{J_f M_1 M(T_e - T_r)}{M_2 C_e x_{mf}(T_e - T_\infty)} + \frac{J_f K_r M_1(T_e - T_r)}{M_2 C_r x_{mf}(T_e - T_\infty)},$$

$$B_{44} \triangleq -\frac{J_f K_r}{C_r x_{mf}} - K_f,$$

$$B_{45} \triangleq \frac{J_f K_e K_r}{M_2 C_e x_{mf}(T_e - T_\infty)^2} + \frac{J_f K_e M(T_r - T_\infty)}{M_2 C_e x_{mf}(T_e - T_r)(T_e - T_\infty)^2} - \frac{J_f M^2}{M_2 C_e x_{mf}(T_e - T_\infty)^2},$$

$$B_{46} \triangleq \frac{J_p K_e M_2(T_e - T_\infty)}{M_1 C_r x_{mp}(T_e - T_r)^2} + \frac{J_f K_e M_1(T_r - T_\infty)}{M_2 C_e x_{mf}(T_e - T_\infty)^2} - \frac{J_f M_1 M(T_e - T_r)}{M_2 C_e x_{mf}(T_e - T_\infty)^2},$$

$$B_{47} \triangleq \frac{J_f K_r M_1(T_e - T_r)}{M_2 C_e x_{mf}(T_e - T_\infty)^2},$$

$$B_{48} \triangleq \frac{J_f K_e^2(T_r - T_\infty)}{M_2 C_e x_{mf}(T_e - T_r)(T_e - T_\infty)^2} - \frac{J_f K_e M}{M_2 C_e x_{mf}(T_e - T_\infty)^2},$$

and

$$B_{49} \triangleq \frac{J_f K_r M}{M_2 C_e x_{mf}(T_e - T_\infty)^2}.$$

Appendix B. Proof of Theorem 1

Let $V(z,t) \in \mathbb{R}$ denote the non-negative function

$$V \triangleq \frac{1}{2} C_e \eta_e^2 + \frac{1}{2} C_r \eta_r^2 + \frac{J_p}{2x_{mp}} \eta_p^2 + \frac{J_f}{2x_{mf}} \eta_f^2, \tag{B.1}$$

where $z \triangleq [\eta_e \ \ \eta_r \ \ \eta_p \ \ \eta_f]^{\mathrm{T}}$. The parameters $\eta_e(t)$, $\eta_r(t)$, $\eta_p(t)$, and $\eta_f(t)$ are defined in Eq. (10). Note that Eq. (B.1) is bounded as (refer to Theorem 2.14 of Qu, 1998) $\lambda_1 \|z(t)\|^2 \leqslant V(z,t) \leqslant \lambda_2 \|z(t)\|^2$ where λ_1 and λ_2 are positive constants. The first time derivative of Eq. (B.1) becomes

$$\begin{aligned}\dot{V} = {} & \eta_e N_e + \eta_r N_r + \eta_p N_p + \eta_f N_f - \eta_e u_e + \eta_r u_r + \eta_p u_p \\ & + \eta_f u_f - M\eta_e\eta_r - M_1(T_e - T_r)\eta_e\eta_p \\ & - M_1(T_e - T_r)\eta_r\eta_p + M_2(T_e - T_\infty)\eta_r\eta_f - C_r\dot{T}_{vr}\eta_r \\ & + \frac{J_p}{x_{mp}}\dot{\omega}_{pd}\eta_p + \frac{J_f}{x_{mf}}\dot{\omega}_{fd}\eta_f,\end{aligned} \tag{B.2}$$

where Eqs. (20)–(22) were utilized. The expressions for $C_r\dot{T}_{vr}(t)\eta_r(t)$, $(J_p/x_{mp})\dot{\omega}_{pd}(t)\eta_p(t)$, and $(J_f/x_{mf})\dot{\omega}_{fd}(t)\eta_f(t)$ can be obtained as

$$C_r\dot{T}_{vr}\eta_r \triangleq \frac{[1+\mathrm{sgn}(u_e)]}{2}F_r, \quad \frac{J_p}{x_{mp}}\dot{\omega}_{pd}\eta_p \triangleq \frac{[\mathrm{sgn}(u_e)-1]}{2}F_p, \quad \frac{J_f}{x_{mf}}\dot{\omega}_{fd}\eta_f \triangleq \frac{[1+\mathrm{sgn}(F)]}{2}F_f, \tag{B.3}$$

where $F(t)$ and $u_e(t)$ were introduced in Eq. (18) and Table 1. The parameters $F_r(t)$, $F_p(t)$, and $F_f(t)$ are defined as

$$\begin{aligned}F_r \triangleq {} & \frac{C_r K_e}{M}\left[\dot{T}_{ed} + \frac{M(T_e - T_{vro}) - Q_{in}}{C_e}\right]\eta_r - \frac{C_r K_e^2}{MC_e}\eta_e\eta_r \\ & - \frac{C_r K_e M_1(T_e - T_r)}{MC_e}\eta_r\eta_p - \frac{C_r K_e}{C_e}\eta_r^2,\end{aligned} \tag{B.4}$$

$$\begin{aligned}F_p \triangleq {} & -\frac{J_p K_e}{M_1 x_{mp}(T_e - T_r)^2}\left[\dot{T}_{ed}(T_e - T_r) + \frac{(T_r - T_{ed})Q_{in}}{C_e} - \frac{M(T_e - T_{vro})(T_r - T_{ed})}{C_e} - \frac{Q_o}{C_r}\eta_e\right]\eta_p \\ & - \frac{J_p K_e}{M_1 x_{mp}}\left[\frac{K_e(T_r - T_{ed})}{C_e(T_e - T_r)^2} + \frac{M}{C_r(T_e - T_r)}\right]\eta_e\eta_p \\ & - \frac{J_p K_e M(T_r - T_{ed})}{M_1 C_e x_{mp}(T_e - T_r)^2}\eta_r\eta_p - \frac{J_p K_e(T_r - T_{ed})}{C_e x_{mp}(T_e - T_r)}\eta_p^2 \\ & - \frac{J_p K_e M_2(T_e - T_\infty)}{M_1 C_r x_{mp}(T_e - T_r)^2}\eta_e\eta_p\eta_f + \frac{J_p K_e}{C_r x_{mp}(T_e - T_r)}\eta_e\eta_p^2 \\ & - \frac{J_p K_e}{M_1 C_r x_{mp}(T_e - T_r)^2}u_r\eta_e\eta_p,\end{aligned} \tag{B.5}$$

$$\begin{aligned}F_f \triangleq {} & \frac{J_f[M_1\dot{\bar{\omega}}_{pd}(T_e - T_r) - \dot{u}_r]}{M_2 x_{mf}(T_e - T_\infty)}\eta_f + \frac{J_f M_1 \bar{\omega}_{pd}}{M_2 C_r x_{mf}(T_e - T_\infty)} \\ & \times [Q_o - M(T_e - T_r) + M_1(T_e - T_r)\eta_p - M_2(T_e - T_\infty)\eta_f - u_r]\eta_f + \frac{J_f[M_1\bar{\omega}_{pd}(T_r - T_\infty) + u_r]}{M_2 C_e x_{mf}(T_e - T_\infty)^2}[Q_{in} \\ & - M(T_e - T_{vro}) + M\eta_r + M_1(T_e - T_r)\eta_p + K_e\eta_e]\eta_f,\end{aligned} \tag{B.6}$$

where the first time derivative of the expressions in Eq. (18) were utilized. The control input, $\bar{\omega}_{pd}(t)$, and control law, $u_r(t)$, are defined in Eq. (18) and Table 1.

The time derivative of the control input is defined as $\dot{\bar{\omega}}_{pd} \triangleq (x_{mp}/2J_p\eta_p)[\mathrm{sgn}(u_e) - 1]F_p$. The derivative, $\dot{u}_r(t)$, is computed based on the control conditions in Table 1. From Eq. (B.3), $C_r\dot{T}_{vr}(t)\eta_r(t)$ and $(J_p/x_{mp})\dot{\omega}_{pd}(t)\eta_p(t)$ change with respect to the sign of the control law $u_e(t)$ as defined in Table 1. Further, $(J_f/x_{mf})\dot{\omega}_{fd}(t)\eta_f(t)$ changes with respect to the sign of the signal $F(t)$ introduced in Eq. (18). Consequently, four cases may be realized as shown in Table B.1.

In Case I, the expression of $\dot{V}(t)$, introduced in Eq. (B.2), can be rewritten as

$$\begin{aligned}\dot{V} = {} & \eta_e N_e + \eta_r N_1 + \eta_p N_p + \eta_f N_f - \eta_e u_e + \eta_r u_r + \eta_p u_p + \eta_f u_f \\ & - M\eta_e\eta_r - M_1(T_e - T_r)\eta_e\eta_p - M_1(T_e - T_r)\eta_r\eta_p \\ & + M_2(T_e - T_\infty)\eta_r\eta_f - C_r\dot{T}_{vr}\eta_r,\end{aligned} \tag{B.7}$$

where

$$N_1 \triangleq \frac{-K_e C_r}{M}\left[\dot{T}_{ed} - \frac{Q_{in}}{C_e} + \frac{M}{C_e}(T_e - T_{vro})\right] + N_r.$$

The variable $N_r(\bullet)$ is defined in Eq. (23). Utilizing the boundedness inequality for $N_r(\bullet)$ and Assumptions A1, A5, and A7, $N_1(\bullet)$ can be upper bounded as $N_1 \leqslant \varepsilon_1$ where ε_1 is a positive constant. Application of the previous bounding inequality, bounding inequalities in Eq. (24), and Table 1 allows the expression for

Table B.1
Four cases for the Lyapunov stability analysis.

Case	Condition	Description		
I	$u_e > 0,\ F \leqslant 0$	$C_r\dot{T}_{vr}(t)\eta_r(t) \neq 0$,	$\frac{J_p}{x_{mp}}\dot{\omega}_{pd}(t)\eta_p(t) = 0$,	$\frac{J_f}{x_{mf}}\dot{\omega}_{fd}(t)\eta_f(t) = 0$
II	$u_e \leqslant 0,\ F \leqslant 0$	$C_r\dot{T}_{vr}(t)\eta_r(t) = 0$,	$\frac{J_p}{x_{mp}}\dot{\omega}_{pd}(t)\eta_p(t) \neq 0$,	$\frac{J_f}{x_{mf}}\dot{\omega}_{fd}(t)\eta_f(t) = 0$
III	$u_e > 0,\ F > 0$	$C_r\dot{T}_{vr}(t)\eta_r(t) \neq 0$,	$\frac{J_p}{x_{mp}}\dot{\omega}_{pd}(t)\eta_p(t) = 0$,	$\frac{J_f}{x_{mf}}\dot{\omega}_{fd}(t)\eta_f(t) \neq 0$
IV	$u_e \leqslant 0,\ F > 0$	$C_r\dot{T}_{vr}(t)\eta_r(t) = 0$,	$\frac{J_p}{x_{mp}}\dot{\omega}_{pd}(t)\eta_p(t) \neq 0$,	$\frac{J_f}{x_{mf}}\dot{\omega}_{fd}(t)\eta_f(t) \neq 0$

$\dot{V}(t)$ in Eq. (B.7) to be upper bounded as

$$\dot{V} \leqslant -\gamma\|z\|^2 + \varepsilon_{ee}|\eta_e| - K_{e2}|\eta_e|^2 + \varepsilon_2|\eta_r| - K_{r2}|\eta_r|^2 + \varepsilon_{pp}|\eta_p| - K_{p2}|\eta_p|^2 + \varepsilon_{ff}|\eta_f| - K_{f2}|\eta_f|^2. \quad \text{(B.8)}$$

In this expression, $z(t)$ was utilized, as well as $\gamma \triangleq \min\{K_{e1}, K_{r1}, K_{p1}, K_{f1}\}$, $K_e \triangleq K_{e1} + K_{e2}$, $K_r \triangleq K_{r1} + K_{r2}$, $K_p \triangleq K_{p1} + K_{p2}$, and $K_f \triangleq K_{f1} + K_{f2}$. By completing the squares for the last eight terms on the right-hand side of (B.8), the following inequality can be obtained (Qu, 1998)

$$\dot{V} \leqslant -\gamma\|z\|^2 + \varepsilon_a, \quad \text{(B.9)}$$

where

$$\varepsilon_a \triangleq \frac{\varepsilon_{ee}^2}{4K_{e2}} + \frac{\varepsilon_1^2}{4K_{r2}} + \frac{\varepsilon_{pp}^2}{4K_{p2}} + \frac{\varepsilon_{ff}^2}{4K_{f2}}.$$

From Eqs. (B.1) and (B.9) and inequality $\lambda_1\|z(t)\|^2 \leqslant V(z,t) \leqslant \lambda_2\|z(t)\|^2$, then $V(z,t) \in L_\infty$. Hence, $\eta_e(t), \eta_r(t), \eta_p(t), \eta_f(t), z(t) \in L_\infty$ and $u_e(t), u_r(t), u_p(t), u_f(t) \in L_\infty$ exist in Table 1 based on Assumptions A2 and A3. Further, the boundedness property of $u_e(t), u_r(t), u_p(t), u_f(t) \in L_\infty$ allows the relationship $\omega_{pd}(t), T_{vr}(t), \omega_{fd}(t), X_p(t), X_f(t) \in L_\infty$ to be realized using Eqs. (18) and (19) in Remark 2 as well as the relations $T_{vr} = T_{vro} + \bar{T}_{vr}$ and $\omega_{pd} \triangleq \bar{\omega}_{pd} + \omega_{po}$. From the previous bounding statements, $T_e(t), T_r(t), \omega_p(t), \omega_f(t), \dot{m}_c(t), \dot{m}_a(t) \in L_\infty$.

For the second and third cases, the expression for $\dot{V}(t)$, introduced in Eq. (B.2), can be rewritten as

$$\dot{V} = \eta_e N_e + \eta_r N_r + \eta_p N_2 + \eta_f N_f - \eta_e u_e + \eta_r u_r + \eta_p u_p + \eta_f u_f - M\eta_e\eta_r - M_1(T_e - T_r)\eta_e\eta_p - M_1(T_e - T_r)\eta_r\eta_p + M_2(T_e - T_\infty)\eta_r\eta_f + \frac{J_p}{x_{mp}}\dot{\omega}_{pd}\eta_p, \quad \text{(B.10)}$$

$$\dot{V} = \eta_e N_e + \eta_r N_3 + \eta_p N_p + \eta_f N_4 - \eta_e u_e + \eta_r u_r + \eta_p u_p + \eta_f u_f - M\eta_e\eta_r - M_1(T_e - T_r)\eta_e\eta_p - M_1(T_e - T_r)\eta_r\eta_p + M_2(T_e - T_\infty)\eta_r\eta_f - C_r\dot{T}_{vr}\eta_r + \frac{J_f}{x_{mf}}\dot{\omega}_{fd}\eta_f. \quad \text{(B.11)}$$

The expression for $\dot{V}(t)$ can be stated for the fourth case as

$$\dot{V} = \eta_e N_e + \eta_r N_r + \eta_p N_5 + \eta_f N_6 - \eta_e u_e + \eta_r u_r + \eta_p u_p + \eta_f u_f - M\eta_e\eta_r - M_1(T_e - T_r)\eta_e\eta_p - M_1(T_e - T_r)\eta_r\eta_p + M_2(T_e - T_\infty)\eta_r\eta_f + \frac{J_p}{x_{mp}}\dot{\omega}_{pd}\eta_p + \frac{J_f}{x_{mf}}\dot{\omega}_{fd}\eta_f. \quad \text{(B.12)}$$

In these three equations, the parameters are

$$N_2 \triangleq N_{21} + N_{22}, \quad N_{21} \triangleq \left(\frac{J_p K_e Q_{in}}{M_1 C_r x_{mp}(T_e - T_r)^2}\right)\eta_e,$$

$$N_{22} \triangleq \frac{J_p K_e}{M_1 x_{mp}(T_e - T_r)}\left[-\frac{Q_{in}(T_r - T_{ed})}{C_e(T_e - T_r)} + \frac{M(T_r - T_{ed})(T_e - T_{vro})}{C_e(T_e - T_r)} - \dot{T}_{ed}\right] + N_{,p},$$

$$N_3 \triangleq K_e C_r\left[\frac{Q_{in}}{MC_e} - \frac{\dot{T}_{ed}}{M} - \frac{(T_e - T_{vro})}{C_e}\right] + N_r, \quad N_4 \triangleq N_{41} + N_{42},$$

$$N_{41} \triangleq \frac{J_f K_e C_r[M(T_e - T_r) - Q_o]}{C_e C_r x_{mf}} + \frac{J_f K_r[M(T_e - T_r) - Q_o]}{C_r x_{mf}} - \frac{J_f K_e K_r \dot{T}_{ed}}{M x_{mf}} + \frac{J_f K_e K_r Q_{in}}{MC_e x_{mf}} - \frac{J_f M_1 \dot{T}_{ed}}{x_{mf}} + \frac{J_f[M_1 Q_{in} - (MM_1 + K_e K_r)(T_e - T_{vro})]}{C_e x_{mf}} + N_f,$$

$$N_{42} \triangleq \left(\frac{J_f(M^2 C_e - K_e^2 C_r)Q_{in}}{M_2 MC_e^2 x_{mf}(T_e - T_\infty)^2}\right)\eta_e - \left(\frac{J_f(K_e C_r + K_r C_e)Q_{in}}{M_2 C_e^2 x_{mf}(T_e - T_\infty)^2}\right)\eta_r,$$

$N_5 \triangleq N_{51} + N_{52}$,

$$N_{51} \triangleq \frac{J_p K_e}{M_1 x_{mp}(T_e - T_r)}\left[\frac{M(T_r - T_{ed})(T_e - T_{vro})}{C_e(T_e - T_r)} - \frac{Q_{in}(T_r - T_{ed})}{C_e(T_e - T_r)} - \dot{T}_{ed}\right] + N_p,$$

$$N_{52} \triangleq \left(\frac{J_p K_e Q_o}{M_1 C_r x_{mp}(T_e - T_r)^2}\right)\eta_e, \quad N_6 \triangleq N_{61} + N_{62},$$

$$N_{61} \triangleq \frac{J_f}{M_2 x_{mf}(T_e - T_\infty)}\left[-K_e(T_e - T_r)\left[M\dot{T}_{ed} + \frac{Q_{in}(T_r - T_{ed})}{C_e(T_e - T_r)} - \frac{M(T_r - T_{ed})(T_e - T_{vro})}{C_e(T_e - T_r)}\right] - \frac{K_r Q_o}{C_r} + \frac{MQ_{in}}{C_e} - M\dot{T}_{ed} - \frac{M^2(T_e - T_{vro})}{C_e} - \frac{K_r M(T_e - T_r)}{C_r}\right] + N_f,$$

Table B.2
Final Lyapunov inequalities for the four cases.

Case	Lyapunov function $V(z,t)$	Definition of λ and ε_a
I	$\dot{V} \leqslant -\gamma\|z\|^2 + \varepsilon_a$	$\gamma \triangleq \min\{K_{e1}, K_{r1}, K_{p1}, K_{f1}\}$, $\varepsilon_a \triangleq \frac{\varepsilon_{ee}^2}{4K_{e2}} + \frac{\varepsilon_1^2}{4K_{r2}} + \frac{\varepsilon_{pp}^2}{4K_{p2}} + \frac{\varepsilon_{ff}^2}{4K_{f2}}$
II	$\dot{V} \leqslant -\gamma\|z\|^2 + \varepsilon_b$	$\gamma \triangleq \min\left\{\left(K_{e1} - \frac{1}{\delta_1}\right), K_{r1}, (K_{p1} - \delta_1), K_{f1}\right\}$, $\varepsilon_b \triangleq \frac{\varepsilon_{ee}^2}{4K_{e2}} + \frac{\varepsilon_{rr}^2}{4K_{r2}} + \frac{\varepsilon_{22}^2}{4K_{p2}} + \frac{\varepsilon_{ff}^2}{4K_{f2}}$
III	$\dot{V} \leqslant -\gamma\|z\|^2 + \varepsilon_c$	$\gamma \triangleq \min\left\{\left(K_{e1} - \frac{1}{\delta_2}\right), \left(K_{r1} - \frac{1}{\delta_3}\right), K_{p1}, (K_{f1} - \delta_2 - \delta_3)\right\}$, $\varepsilon_c \triangleq \frac{\varepsilon_{ee}^2}{4K_{e2}} + \frac{\varepsilon_3^2}{4K_{r2}} + \frac{\varepsilon_{pp}^2}{4K_{p2}} + \frac{\varepsilon_{41}^2}{4K_{f2}}$
IV	$\dot{V} \leqslant -\gamma\|z\|^2 + \varepsilon_d$	$\gamma \triangleq \min\left\{\left(K_{e1} - \frac{1}{\delta_4} - \frac{1}{\delta_5}\right), \left(K_{r1} - \frac{1}{\delta_6}\right), (K_{p1} - \delta_4), (K_{f1} - \delta_5 - \delta_6)\right\}$, $\varepsilon_d \triangleq \frac{\varepsilon_{ee}^2}{4K_{e2}} + \frac{\varepsilon_{rr}^2}{4K_{r2}} + \frac{\varepsilon_{51}^2}{4K_{p2}} + \frac{\varepsilon_{61}^2}{4K_{f2}}$

and

$$N_{62} \triangleq -\left(\frac{J_f K_r Q_{in}}{M_2 C_e x_{mf}(T_e - T_\infty)^2}\right)\eta_r + \left(\frac{J_f}{M_2 x_{mf}(T_e - T_\infty)^2}\left[\frac{MQ_{in}}{C_e} - \frac{K_e Q_{in}(T_r - T_\infty)}{C_r(T_e - T_r)}\right]\right)\eta_e.$$

Utilizing the boundedness inequalities for $N_r(\bullet)$, $N_p(\bullet)$, and $N_f(\bullet)$ in Eq. (23) and Assumptions A1–A3, A5, and A6, the terms $N_{21}(\bullet)$, $N_{22}(\bullet)$, $N_3(\bullet)$, $N_{41}(\bullet)$, $N_{42}(\bullet)$, $N_{51}(\bullet)$, $N_{52}(\bullet)$, $N_{61}(\bullet)$, and $N_{62}(\bullet)$ can be upper bounded as $N_{21} \leqslant \varepsilon_{21}|\eta_e|$, $N_{22} \leqslant \varepsilon_{22}$, $N_3 \leqslant \varepsilon_3$, $N_{41} \leqslant \varepsilon_{41}$, $N_{42} \leqslant \varepsilon_{42a}|\eta_e| + \varepsilon_{42b}|\eta_r|$, $N_{51} \leqslant \varepsilon_{51}$, $N_{52} \leqslant \varepsilon_{52}|\eta_e|$, $N_{61} \leqslant \varepsilon_{61}$, and $N_{62} \leqslant \varepsilon_{62a}|\eta_e| + \varepsilon_{62b}|\eta_r|$, respectively. Note that the parameters ε_{21}, ε_{22}, ε_3, ε_{41}, ε_{42a}, ε_{42b}, ε_{51}, ε_{52}, ε_{61}, ε_{62a}, and ε_{62b} are positive constants.

Application of the previous bounding inequalities, Eq. (23), and Table 1 allows $\dot{V}(t)$ to be upper bounded in Table B.2. The inequalities

$$\varepsilon_{21}|\eta_e||\eta_p| \leqslant \frac{1}{\delta}|\eta_e|^2 + \delta|\eta_p|^2,$$

$$\varepsilon_{42a}|\eta_e||\eta_f| \leqslant \frac{1}{\delta_2}|\eta_e|^2 + \delta_2|\eta_f|^2,$$

$$\varepsilon_{42b}|\eta_r||\eta_f| \leqslant \frac{1}{\delta_3}|\eta_r|^2 + \delta_3|\eta_f|^2,$$

$$\varepsilon_{52}|\eta_e||\eta_p| \leqslant \frac{1}{\delta_4}|\eta_e|^2 + \delta_4|\eta_p|^2,$$

$$\varepsilon_{62a}|\eta_e||\eta_f| \leqslant \frac{1}{\delta_5}|\eta_e|^2 + \delta_5|\eta_f|^2,$$

and

$$\varepsilon_{62b}|\eta_r||\eta_f| \leqslant \frac{1}{\delta_6}|\eta_r|^2 + \delta_6|\eta_f|^2$$

were utilized as well as the definitions of K_e, K_r, K_p, and K_f in Case I. For Case II, $K_{e1} \geqslant 1/\delta_1$ and $K_{p1} \geqslant \delta_1$. In Case III, $K_{e1} \geqslant 1/\delta_2$, $K_{r1} \geqslant 1/\delta_3$, and $K_{f1} \geqslant \delta_2 + \delta_3$. In Case IV, $K_{e1} \geqslant 1/\delta_4 + 1/\delta_5$, $K_{r1} \geqslant 1/\delta_6$, $K_{p1} \geqslant \delta_4$, and $K_{f1} \geqslant \delta_5 + \delta_6$. For all cases, $\delta_i \forall i = 1, 2, \ldots, 6$ are positive constants. Finally, similar argument as in Case I can show that all signals are bounded for the Cases II–IV to conclude the inequality in Eq. (B.9).

References

Allen, D., & Lasecki, M. (2001). *Thermal management evolution and controlled coolant flow*. SAE technical paper no. 2001-01-1732.

Chastain, J., & Wagner, J. (2006). *Advanced thermal management for internal combustion engines-valve design, component testing and block redesign*. SAE paper no. 2006-01-1232, April 2006.

Chen, J., Dixon, W., Wagner, J., & Dawson, D. (2002). Exponential tracking control of a hydraulic proportional directional valve and cylinder via integrator backstepping. In *Proceedings of the ASME IMECE, dynamics systems and control division*, IMECE2002-32076, New Orleans, LA, November 2002.

Chiang, M., Lee, L., & Huang, K. (2005). Development of a hydraulic-piezoelectric-actuator for hybrid positioning control with large stroke, high loading and sub-micrometer accuracy. In *Proceedings of the IEEE international conference on mechatronics* (pp. 45–49), Taipei, Taiwan, July 2005.

Choukroun, A., Chanfreau, M. (2001). *Automatic control of electric actuators for an optimized engine cooling thermal management*. SAE technical paper no. 2001-01-1758.

Dostal, G. (1994). *Hydraulic power and cooling capacity available from agricultural tractors for operating hydraulic motors*. MS Thesis, Department of Mechanical Engineering, Iowa State University.

Frick, P., Bassily, H., Watson, H., & Wagner, J. (2006). A hydraulic fan driven heat exchanger for automotive cooling systems. In *Proceedings of the ASME IMECE, dynamics systems and control division*, IMECE2006-13464, Chicago, IL, November 2006.

Hamamoto, T., Omura, S., Ishikawa, N., & Sugiyama, T. (1990). *Development of the electronically controlled hydraulic cooling fan system*. SAE technical paper no. 901710.

Havlicsek, H., & Alleyne, A. (1999). Nonlinear control of an electrohydraulic injection molding machine via iterative adaptive learning. *IEEE/ASME Transactions on Mechatronics*, *4*(3), 312–323.

Henry, R., Koo, J., & Richter, C. (2001). *Model development, simulation and validation, of power train cooling system for a truck application*. SAE technical paper no. 2001-01-1731.

Kaddissi, C., Kenné, J.-P., & Saad, M. (2007). Identification and real-time control of an electrohydraulic servo system based on nonlinear backstepping. *IEEE/ASME Transactions on Mechatronics*, *12*(1), 12–22.

Liu, R., & Alleyne, A. (2000). Nonlinear force/pressure tracking of an electro-hydraulic actuator. *ASME Journal of Dynamic Systems, Measurement, and Control*, *122*(1), 232–237.

Merritt, H. (1967). *Hydraulic control systems*. New York: Wiley.

Qu, Z. (1998). *Robust control of nonlinear uncertain systems*. New York: Wiley.

Salah, M., Mitchell, T., Wagner, J., & Dawson, D. (2008). Nonlinear control strategy for advanced vehicle thermal management systems. *IEEE Transactions on Vehicular Technology*, *57*(1), 127–137.

Setlur, P., Wagner, J., Dawson, D., & Marotta, E. (2005). An advanced engine thermal management system: Nonlinear control and test. *IEEE/ASME Transactions on Mechatronics*, *10*(2), 210–220.

Shaver, G., Roelle, M., & Gerdes, J. (2006). Modeling cycle-to-cycle dynamics and mode transition in HCCI engines with variable valve actuation. *Control Engineering Practice*, *14*(3), 213–222.

Vaughan, N., & Gamble, J. (1996). The modeling and simulation of a proportional solenoid valve. *ASME Journal of Dynamic Systems, Measurement, and Control*, *118*(1), 120–125.

Wagner, J., Paradis, I., Marotta, E., & Dawson, D. (2002). Enhanced automotive engine cooling systems—a mechatronics approach. *International Journal of Vehicle Design*, *28*(1–3), 214–240.

Wambsganss, M. (1999). *Thermal management concepts for higher-efficiency heavy vehicle*. SAE technical paper no. 1999-01-2240.

Yao, B., Bu, F., & Chiu, G. (2001). Nonlinear adaptive robust control of electro-hydraulic systems driven by double-rod actuators. *International Journal of Control*, *74*(8), 761–775.

Yao, B., Bu, F., Reedy, J., & Chiu, G. (2000). Adaptive robust motion control of single-rod hydraulic actuators: Theory and experiments. *IEEE/ASME Transactions on Mechatronics*, *5*(1), 79–91.